



“Turn-On” Fluorescent Biosensors for High Selective and Sensitive Detection of Al³⁺ Ion

Pengfei Wang¹, Lijie Liu¹, Fanda Meng², Maroof Ahmad Khan¹ and Hui Li^{1*}

¹ Key Laboratory of Cluster Science of Ministry of Education, School of Chemistry and Chemical Engineering, Beijing Institute of Technology, Beijing, China, ² Institute of Basic Medicine, Shandong First Medical University & Shandong Academy of Medical Sciences, Shandong, China

OPEN ACCESS

Edited by:

Guangle Niu,
Shandong University, China

Reviewed by:

Hai-Tao Feng,
Baoji University of Arts and
Sciences, China
Xuechen Li,
Qilu University of Technology, China
Xiujuan Shi,
Hong Kong University of Science and
Technology, Hong Kong

*Correspondence:

Hui Li
lihui@bit.edu.cn

Specialty section:

This article was submitted to
Analytical Chemistry,
a section of the journal
Frontiers in Chemistry

Received: 17 September 2020

Accepted: 05 October 2020

Published: 19 November 2020

Citation:

Wang P, Liu L, Meng F, Khan MA and
Li H (2020) “Turn-On” Fluorescent
Biosensors for High Selective and
Sensitive Detection of Al³⁺ Ion.
Front. Chem. 8:607614.
doi: 10.3389/fchem.2020.607614

A series of new compounds (**1-4**) based on pyrrole hydrazone Schiff bases were designed and synthesized. The interactions of these new compounds with metal ions and their fluorescent recognition were investigated. All compounds showed “turn-on” fluorescence in the presence of Al³⁺ in aqueous solution. Their sensing behaviors with Al³⁺ were studied using photophysical experiments, ESI-MS spectrometry analysis, ¹H NMR titration, and DFT calculation. The detection limits of **1-4** for the analysis of Al³⁺ were found to reach a 10⁻⁸ M level in aqueous solution, which are far lower than the WHO guidelines for drinking water (7.41 mM for Al³⁺). A high selectivity test paper has been fabricated for Al³⁺ detection based on sensor **3**. Theoretical calculations (DFT) have been carried out to elucidate the configuration of **1-4** and their Al complexes and rationalize experimental absorption data.

Keywords: pyrrole hydrazone Schiff base, fluorescent biosensors, detection of Al³⁺, theoretical calculation, test paper

INTRODUCTION

Aluminum is widely used as a common metal, the content is second only to oxygen and silicon, ranking third, and is the most abundant metal element in the Earth's crust (Das et al., 2013; Sahana et al., 2013). Aluminum and its compounds have been widely used in food additives (Aguilar et al., 2008; Kim et al., 2012), water treatment, pharmaceuticals, and light alloy production (DeVoto and Yokel, 1994; Greger et al., 1997; Berthon, 2002). The toxic effects of Al³⁺ ions not only affect plants and aquatic ecosystems, but they also affect humans. Long-term exposure to aluminum can cause harm to human bodies and organs including the onset of diseases such as Alzheimer's disease and Parkinson's disease, and memory loss and cardiac arrest (Liao et al., 2013; Chatterjee et al., 2016; Kumawat et al., 2016; Liu et al., 2016) or even threaten life. Aluminum products were listed in the first category of carcinogens as a preliminary list of carcinogens. According to the World Health Organization's assessment, the daily intake of aluminum is specified to be 3–10 mg/day, and the limits of Al³⁺ concentration in drinking water is 7.41 mM (Valeur and Leray, 2000; Barcelo and Poschenrieder, 2002; Krejpcio and Wojciak, 2002). Fluorescence sensors have generated extensive research in the past few decades, due to their simple operation (Kong et al., 2014; Singh et al., 2017; Sharma et al., 2019; Shi et al., 2020), extremely high sensitivity (Dong et al., 2017; Fu J. et al., 2019; Li et al., 2020), and direct visual effect (Fu W. et al., 2019; Tang et al., 2019; Jiao et al., 2020) and high selectivity (Li X. et al., 2014; Jiang et al., 2017). Most Al³⁺ sensors are designed with quite complex structures, which are difficult to synthesize and dissolve in water (Li et al., 2013; Li T. et al., 2014; Gupta and Kumar, 2016; Huang et al., 2016; Balakrishnan et al., 2017). Therefore, it is necessary to

develop a water-soluble Al³⁺ sensor that can be easily synthesized and can detect Al³⁺ with high selectivity in aqueous environments even at very low concentrations.

The hydrazone Schiff base has been widely investigated for convenient synthesis, adjustable electronic properties, and excellent chelating ability (Boonkitpatarakul et al., 2015). The thiophene- and furan-hydrazone Schiff bases have been used as fluorescent sensors for metal ions, anions, and organic acids (Boonkitpatarakul et al., 2015; Hwang et al., 2017; Jeong et al., 2017). In addition, diethylaminophenol has also been selected as an ideal component of many chemical sensors because it is a well-known chromophore that has hydrophilic properties and functions (Aguilar et al., 2008; Jeong et al., 2017). However, pyrrole hydrazone Schiff bases, as a common heterocyclic compound are rarely studied. A pyrrole hydrazone Schiff base also has potential application value in ion recognition owing to its hydrazone structure. Our group has reported some research results in the field of fluorescence detection in the early stage (Hao et al., 2016; Song et al., 2020). In this work, we reported a series of chemosensors based on pyrrole hydrazone Schiff base derivatives (**Scheme 1**). Sensor **1** was synthesized referring to a literature method (Hanna et al., 2007). Our study found that it had a high selectivity Al³⁺ fluorescence recognition property. We look forward to designing and changing its structure with **1** as the core structure, so that the emission spectrum can be shifted to longer wavelengths, but its high-efficiency ion recognition properties are not affected. We designed and synthesized sensors **2** and **3** as the electron-donating substituents N, N-diethyl and methoxy groups were introduced to the benzene ring, which were beneficial to improve HOMO level of molecules. The strategy of extensive π -conjugation was applied in sensor **4** by replacing the benzene ring with a naphthalene ring. We expect that the designed sensors 2-4 have more efficient and selective fluorescence recognition properties for Al³⁺ and have more responsive long-wave colors in the emission spectrum.

EXPERIMENTAL SECTION

Materials

All solvents and reagents (analytical and spectral) were obtained from Sigma-Aldrich and used as standard.

Measurements and Instruments

¹H NMR and ¹³C NMR measurements were performed on a Bruker AVANCE III HD 400 MHz nuclear magnetic resonance spectrometer, the ¹H-¹H COSY NMR spectrum were performed on a Bruker AVANCE III HD 700 MHz nuclear magnetic resonance spectrometer. Electrospray ionization mass spectrometry (ESI-MS) was collected on an AGILENT Q-TOF 6520 LC-MS instrument. Absorption spectra were collected at room temperature using a PERSEE TU-1950 double-beam UV-Vis spectrophotometer. The fluorescence emission spectrum was collected on a HITACHI F-7000 fluorescence spectrophotometer. Absolute PL quantum yield was collected using a Quantaaurus-QY Absolute PL quantum yield spectrometer C11347-11 | Hamamatsu Photonics. IR spectrums were collected using a Thermo IS5 Fourier transform infrared spectrometer. Elemental

analysis of carbon, nitrogen, and hydrogen was performed using an EA3000 elemental analyzer at the Analysis and Testing Center of Beijing Institute of Technology.

Preparation of Compounds

1H-Pyrrole-2-carbohydrazide

N₂H₄·H₂O (80% in water, 30 ml) and 1H-pyrrole-2-carboxylic acid ethyl ester (10 g) was added to a 100 ml Schlenk flask. After vacuumizing and filling with nitrogen three times, the reaction was placed in a 70°C oil bath and kept for 12 h (Pawel et al., 2009). After the reaction, the resulting reaction suspension was filtered and washed with cold water to obtain 8.5 g (94%) of the product as colorless crystals, ¹H NMR (400 MHz, DMSO-*d*₆) δ 11.42 (s, 1H), 9.22 (s, 1H), 6.83 (td, *J* = 2.7, 1.4 Hz, 1H), 6.73 (ddd, *J* = 3.9, 2.5, 1.5 Hz, 1H), 6.05 (dt, *J* = 3.7, 2.4 Hz, 1H), 4.28 (s, 2H).

A typical synthesis of sensors **1-4** was performed by refluxing a mixture of o-hydroxybenzaldehyde (1.0 mmol) and 1H-pyrrole-2-carbohydrazide (1.01 mmol) in 10 mL of methanol for 24 h. The resulting mixture was cooled down to room temperature. The precipitate was filtered off and washed with cold methanol and cold water. The resulting solid products were obtained by characterization by ¹H NMR, ¹³C NMR, and HRMS.

(E)-N'-(2-hydroxybenzylidene)-1H-pyrrole-2-carbohydrazide (**1**)

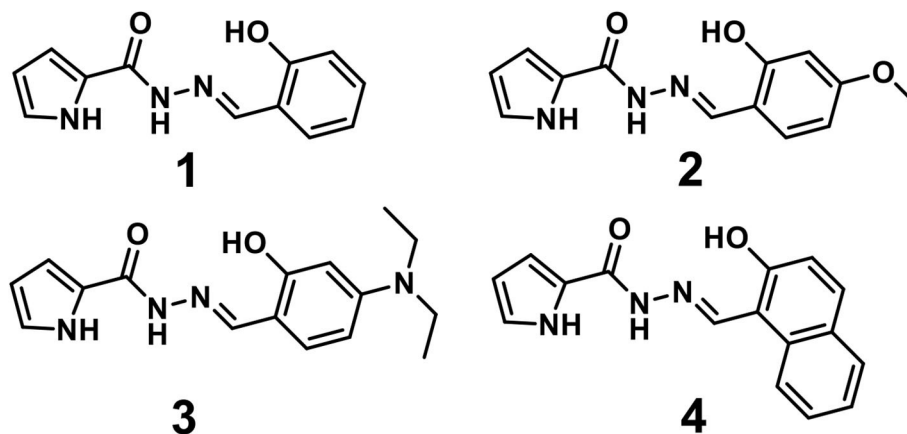
The precipitate was collected in 96% yield as white powder. ¹H NMR (400 MHz, DMSO-*d*₆) δ 11.76 (s, 1H), 11.71 (s, 1H), 11.31 (s, 1H), 8.53 (s, 1H), 7.64–7.46 (m, 1H), 7.28 (t, *J* = 6.9 Hz, 1H), 7.00 (d, *J* = 1.4 Hz, 2H), 6.91 (t, *J* = 7.3 Hz, 2H), 6.18 (dt, *J* = 3.6, 2.4 Hz, 1H) ppm. ¹³C NMR (176 MHz, DMSO-*d*₆) δ 157.42, 157.15, 146.74, 131.35, 129.61, 124.24, 123.48, 119.68, 119.07, 116.60, 111.68, 109.50. HRMS calcd. C₁₂H₁₁N₃O₂ 229.0851, calcd. C₁₂H₁₂N₃O₂⁺ 230.0924, found M+H⁺ 230.0914.

(E)-N'-(2-hydroxy-4-methoxybenzylidene)-1H-pyrrole-2-carbohydrazide (**2**)

The precipitate was collected in 92% yield as white powder. ¹H NMR (400 MHz, DMSO-*d*₆) δ 11.72 (s, 1H), 11.63 (s, 1H), 11.60 (s, 1H), 8.45 (s, 1H), 7.41 (d, *J* = 6.9 Hz, 1H), 6.99 (s, 1H), 6.96 (s, 1H), 6.52 (d, *J* = 8.5 Hz, 1H), 6.49 (s, 1H), 6.18 (s, 1H), 3.77 (s, 3H) ppm. ¹³C NMR (176 MHz, DMSO-*d*₆) δ 162.22, 159.62, 157.11, 147.34, 131.33, 124.68, 123.35, 112.48, 111.55, 109.52, 106.78, 101.64, 55.74. HRMS calcd. C₁₃H₁₄N₃O₃ 260.1035, found M+H⁺ 260.1023; calcd. C₁₃H₁₃N₃O₃Na 282.0844, found M+Na⁺ 282.0844.

(E)-N'-(4-(diethylamino)-2-hydroxybenzylidene)-1H-pyrrole-2-carbohydrazide (**3**)

The precipitate was collected in 95% yield as light yellow powder. ¹H NMR (400 MHz, DMSO-*d*₆) δ 11.66 (s, 1H), 11.45 (s, 1H), 11.40 (s, 1H), 8.34 (s, 1H), 7.18 (d, *J* = 7.5 Hz, 1H), 6.96 (s, 1H), 6.92 (s, 1H), 6.26 (d, *J* = 8.6 Hz, 1H), 6.16 (s, 1H), 6.12 (s, 1H), 1.10 (t, *J* = 6.6 Hz, 6H) ppm. ¹³C NMR (101 MHz, DMSO-*d*₆) δ 159.92, 156.90, 150.36, 148.66, 131.76, 124.93, 123.00, 111.16, 109.42, 107.19, 104.05, 98.04, 44.26, 13.00. HRMS calcd. C₁₆H₂₁N₄O₂ 301.1659, found M+H⁺ 301.1657; calcd. C₁₆H₂₀N₄O₂Na 323.1478, found M+Na⁺ 323.1483.



SCHEME 1 | The illustration of molecular structures of sensors 1-4.

(*E*)-*N'*-((2-hydroxynaphthalen-1-yl)methylene)-1*H*-pyrrole-2-carbohydrazide(4)

The precipitate was collected in 90% yield as yellow powder. ¹H NMR (400 MHz, DMSO-*d*₆) δ 12.85 (s, 1H), 11.87 (s, 1H), 11.85 (s, 1H), 9.40 (s, 1H), 8.22 (d, *J* = 8.6 Hz, 1H), 7.91 (t, *J* = 8.1 Hz, 2H), 7.61 (t, *J* = 7.7 Hz, 1H), 7.42 (t, *J* = 7.5 Hz, 1H), 7.24 (d, *J* = 8.9 Hz, 1H), 7.08–7.04 (m, 1H), 7.02 (s, 1H), 6.25 (d, *J* = 3.0 Hz, 1H). ¹³C NMR (176 MHz, DMSO-*d*₆) δ 158.07, 157.00, 145.21, 132.73, 131.97, 129.42, 128.27, 128.11, 124.51, 123.94, 123.71, 121.02, 119.36, 111.69, 109.68, 109.17. HRMS calcd. C₁₆H₁₃N₃O₂ 279.1008, calcd. C₁₆H₁₄N₃O₂⁺ 280.1081, found M+H⁺ 280.1080; calcd. C₁₆H₁₃N₃NaO₂⁺ 302.0900, found M+Na⁺ 302.0909.

UV-Vis Titration Experiments

A solution of sensors 1-4 (3 mM) in DMSO was prepared, and 10 μL sensors 1-4 (3 mM) was diluted with a 2.990 mL bis-tris buffer solution (PH = 7.4) to bring the final concentration to 10 μM. Then, 1-10 uL of Al(NO₃)₃ solution (3 mM) was added to the 3 mL of 1-4 solution (10 μM). After mixing for 1 min, UV-Vis absorption spectra were performed at room temperature.

Fluorescence Titration Experiments

A solution of sensors 1-4 (3 mM) in DMSO was prepared, and 1 μL of sensors 1-4 (3 mM) was diluted with a 2.999 mL bis-tris buffer solution (PH = 7.4) to bring the final concentration to 1 μM. Then, 0.1-1 μL of Al(NO₃)₃ solution (3 mM) was added to the 3 mL of 1-4 solution (1 μM). After mixing for 1 min, fluorescence spectra were performed at room temperature.

Job's Plot Measures

Bis-tris solutions of sensors 1-4 (10 μM) and Al(NO₃)₃ (10 μM) of the same concentration were prepared, respectively, and then a series of mixed solutions containing sensors 1-4 and Al(NO₃)₃ were prepared to keep the total volume of the solution at 3 mL. The volume ratio of the sensors and Al³⁺ ion are 10:0, 9:1, 8:2, 7:3, 6:4, 5:5, 4:6, 3:7, 2:8, 1:9, 0:10. After mixing for a few minutes, the fluorescence spectrum was acquired at room temperature.

Job's Plot was drawn by plotting the fluorescence intensity and the ratio of sensor to ion volume.

Competition Experiments

A solution of sensors 1-4 (3 mM) in DMSO was prepared, and 1 μL of sensors 1-4 (3 mM) was diluted with a 2.999 mL bis-tris buffer solution (PH = 7.4) to bring the final concentration to 1 μM. Solutions of various metal ions (4.5 μL, 20 mM, 30 equivalents) including Na⁺, K⁺, Ag⁺, Mg²⁺, Ca²⁺, Hg²⁺, Pb²⁺, Cd²⁺, Mn²⁺, Ni²⁺, Co²⁺, Cu²⁺, Zn²⁺, Fe²⁺, Fe³⁺, and Cr³⁺ were added to each sensor 1-4 solution (3 mL, 1 μM). The Al(NO₃)₃ 9H₂O solution (4.5 mL, 20 mM, 30 equivalent) was then added to the above solutions. After mixing for 5 min, fluorescence spectra were taken at room temperature.

¹H NMR Titration

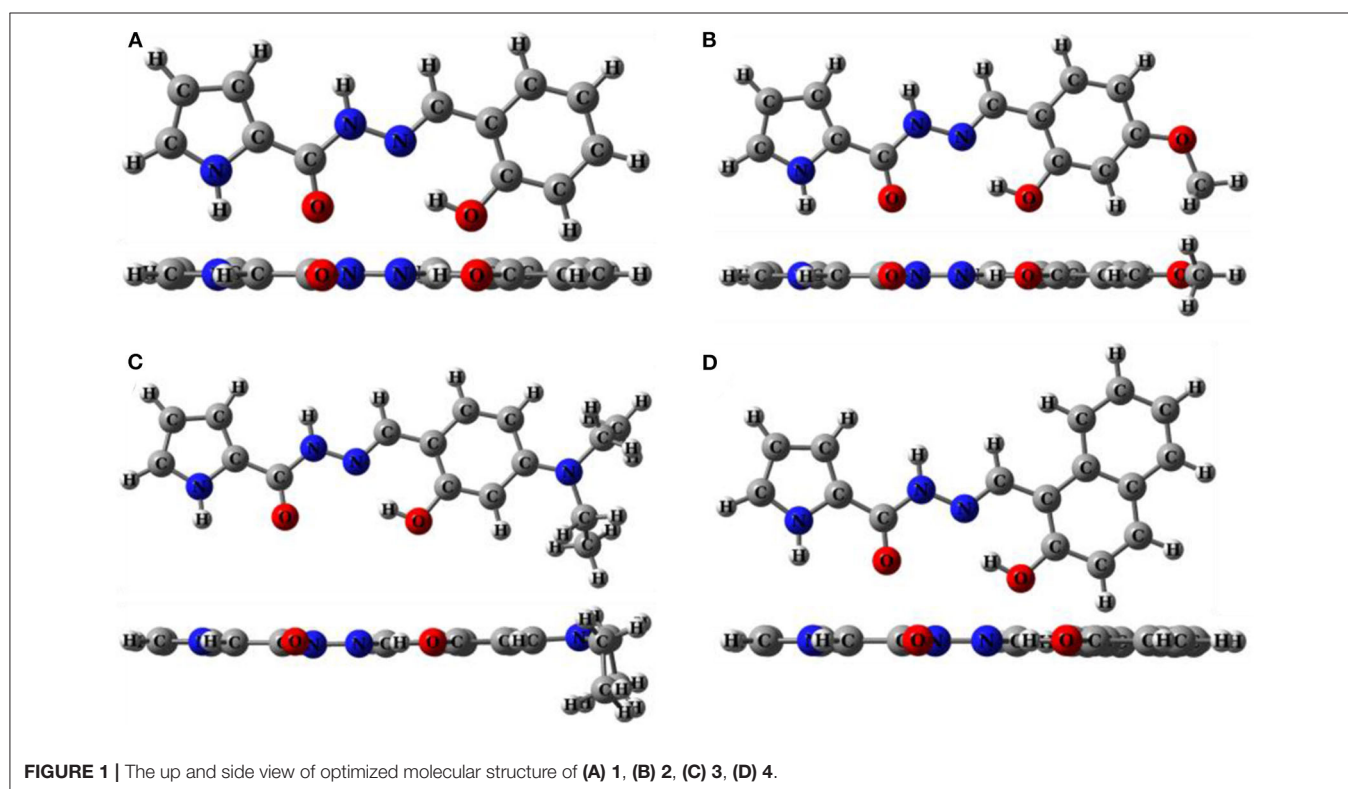
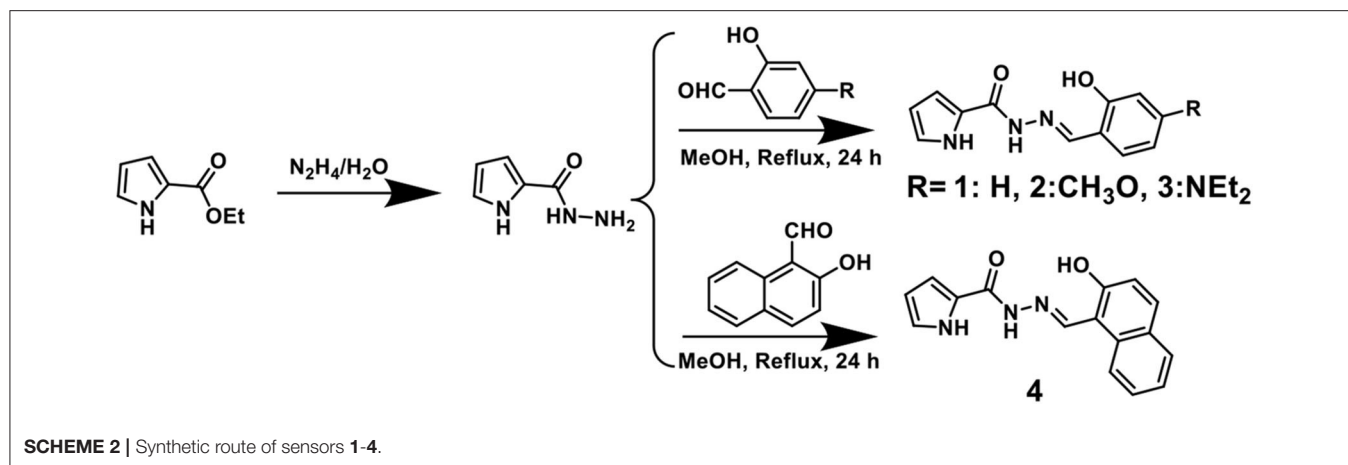
Three NMR samples of sensor 3 (3.01 mg, 0.01 mmol) were dissolved in DMSO-*d*₆ (500 μL), and three different amounts of Al(NO₃)₃ solutions (0, 0.5, and 1.0 eq.) were added to each sample. After the mixtures were mixed for 30 min, ¹H NMR spectroscopy was performed at room temperature.

Theoretical Calculation

DFT and TD-DFT calculations were operated by the Gaussian 09 software (Frisch et al., 2009) at the B3LYP/6-31G(d) level. The input files and orbital representations were generated with Gaussview 5.0 (scaling radii of 75%, isovalue of 0.05). Geometries and electronic properties were calculated by means of hybrid density functional B3LYP with the basis set of 6-31G(d). GaussSum 3.0 (O'Boyle et al., 2008) was used to calculate the contribution of molecular orbitals (MO) in electronic transitions and the theoretical absorption spectrum.

Fluorescence Test Paper Detector

In order to facilitate rapid detection and analysis, a paper-based fluorescence sensor for Al³⁺ detection was developed. A series of circular test papers with a diameter of 0.5 cm were prepared by adding 10 μL of 10 μM sensor 3 solution, and then dried to make Al³⁺ test papers. Then 10 μL and 10 μM of different metal ions



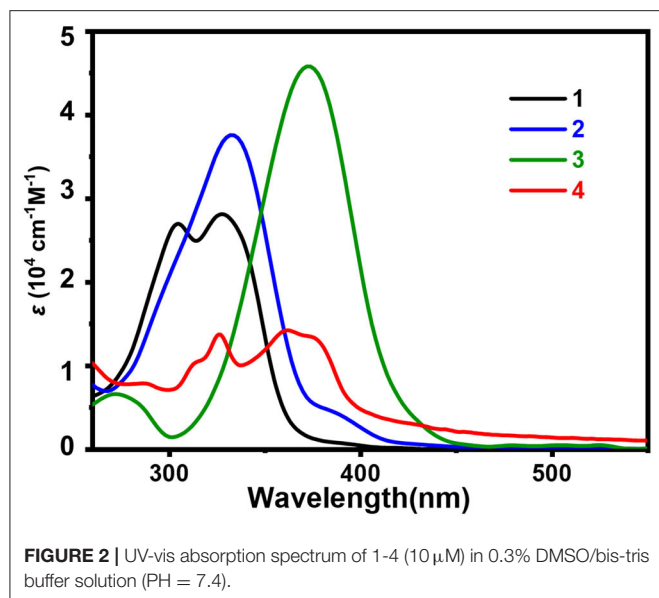
(Na⁺, K⁺, Ag⁺, Mg²⁺, Ca²⁺, Hg²⁺, Pb²⁺, Cd²⁺, Mn²⁺, Ni²⁺, Co²⁺, Cu²⁺, Zn²⁺, Fe²⁺, Fe³⁺, and Cr³⁺) were added to each test paper.

RESULTS AND DISCUSSION

Synthesis of Sensors 1-4

As shown in **Scheme 2**, sensors 1-4 were synthesized easily from *o*-hydroxybenzaldehyde derivatives and 1*H*-pyrrole-2-carbohydrazide via a one-step condensation reaction with high yields ($\geq 90\%$). Sensors 1-4 have good solubility in many common solvents, such as methanol,

ethanol, DMSO, and DMF, and it is also slightly soluble in water. These compounds were fully characterized by ¹H NMR, ¹³C NMR, and HRMS (**Supplementary Figures 2–13**). The geometries of 1-4 were optimized by DFT calculations. The up and side views of the optimized molecular structure of 1-4 with atomic tags are shown in **Figure 1**. Due to the good conjugation in these molecules, the pyrrole ring, acylhydrazone, and benzene ring are almost on the same plane, which makes them have excellent planarity, and it is conducive to the intramolecular PET effect. Therefore, 1-4 aqueous solutions showed very weak fluorescence intensity.



UV-Vis Absorption Studies

In the research for the investigation of sensing property, the absorption spectrum of sensors is an essential photophysical property. All of the absorption spectra were recorded in aqueous solution (about 0.3% DMSO) at room temperature. The data are summarized and shown in **Figure 2** and **Table 1**. The UV-Vis absorption spectrum of compounds **1-4** in aqueous solution (0.3% DMSO) is shown in **Figure 2**. The figure shows two main absorption bands, corresponding to $\pi-\pi^*$ and $n-\pi^*$ transitions, respectively. The maximum absorption peaks of compounds **1-4** are 328, 333, 372, and 376 nm, respectively. Compared with **1**, the maximum absorption peaks of compounds **2-4** all show clear red shifts. However, the maximum absorption peaks of compounds **3** and **4** show large red shifts (44 and 48 nm, respectively), this may due to the additional donor group (N, N-diethyl) (**3**) and extended π conjugation (**4**). The absorption spectrum of **2** only shows a small amount of red shift (5 nm) owing to the electron donating ability of the methoxy group is weaker than that of the N, N-diethyl group. As shown in the absorption spectrum obtained by theoretical calculations of **1-4** (**Supplementary Figure 22**), the maximum absorption peaks of compounds **1-4** are 334, 339, 370, and 373 nm. Compared with **1**, the maximum absorption peaks of **2**, **3**, and **4** show obvious red shifts. The amounts of red shift are almost the same as the data obtained by the experiment.

UV-vis titration analysis was performed by gradually adding Al³⁺ ions (0-1 eq.) to compounds **1-4**, respectively. As shown in **Figure 3**, each compound absorption band has a significant change with the gradual increase of Al³⁺ ion content. Compound **1** has two new absorption bands near 325 nm and 375 nm, and absorption bands near 300 and 325 nm gradually decreasing, there are two equivalent absorption points at 256 and 350 nm; **2** has two new absorption bands near 310 and 380 nm, the absorption band near 333 nm gradually decreases, the equal absorption points are at 275 and 360 nm; **3** has two new

TABLE 1 | Photophysical data of 1-4 with and without Al³⁺ in aqueous solution.

Compound	Absorption ^a	Emission ^b	
	λ_{\max} (nm), ϵ ($10^4 \text{ cm}^{-1} \text{ M}^{-1}$)	λ_{\max} (nm)	Φ
1	328 (2.7)	429	0.012
2	333 (3.8)	430	0.015
3	372 (4.6)	445	0.011
4	376 (1.3)	472	0.042
1-Al	387 (2.1)	446	0.199
2-Al	395 (2.4)	448	0.314
3-Al	417 (2.6)	453	0.315
4-Al	425 (1.2)	480	0.093

^a Measured in 0.3% DMSO/bis-tris buffer solution (PH = 7.4) at 1.0×10^{-5} M, RT.

^b Recorded in 0.03% DMSO/bis-tris buffer solution (PH = 7.4) at 1.0×10^{-6} M.

absorption bands at 275 and 398 nm, the absorption band near 372 nm gradually decreases with an equivalent point near 390 nm; and **4** has three new absorption bands at 340, 402, and 425 nm. The absorption bands around 325 and 376 nm gradually decrease, and the equivalent absorption points are at 276 and 380 nm, respectively. These bands are attributed to the $\pi-\pi^*$ transition of the pyrrole unit and the charge transfer transition in the Al³⁺ complexes. The existence of the equivalent absorption points indicates that coordination interactions exist between the ligands **1-4** and Al³⁺ ion.

Interaction Between Sensors and Al³⁺

With the addition of Al³⁺ from 0 to 1.0 eq., the new absorption peaks of compounds **1-4** at 372 nm, 385, 398, and 425 nm increase linearly (**Figure 3**). This result indicates that **1-4** can be used for quantitative analysis of Al³⁺. When the amount of Al³⁺ added exceeds 1 eq., the weak increase in peak intensity indicates that the binding mode of the sensors **1-4** toward Al³⁺ follows a 1:1 stoichiometric ratio.

According to the calculation of equation $\text{LOD} > 3\sigma/k$, the detection limits of sensors **1-4** for Al³⁺ are 53, 45, 42, and 102 nM, where σ is the standard deviation of the blank measurement, and k is the slope of the calibration line (**Supplementary Figure 16**). Using the Benesi-Hildebrand expression, the association constants (K_a) of **1-4** were calculated to be approximately 4×10^4 , 5.3×10^4 , 4.5×10^4 , and 1.1×10^4 (**Supplementary Figure 17**). The comparative analysis of sensors **1-4** with previously reported sensors are shown in **Supplementary Table 1**.

In order to confirm the binding mode of **1-4** toward Al³⁺, Job's Plot for fluorescence was carried out (**Supplementary Figure 18**). The maximum fluorescence intensity of **1-4** were reached at a molar fraction of 0.5, indicating a 1:1 ratio for the Al³⁺ complexes of **1-4**. Furthermore, the ESI mass spectra of **1-4** in the presence of Al³⁺ were also measured (**Figure 4**), which is regarded as direct evidence for understanding the binding mode between metal ions and sensors. The ESI-MS peaks at m/z 317.0415, 347.0599, 388.1197, and 367.0618, corresponding to $[\text{AlNO}_3 \cdot (\text{1-H})]^+$ (calcd = 317.0461), $[\text{AlNO}_3 \cdot (\text{2-H})]^+$ (calcd =

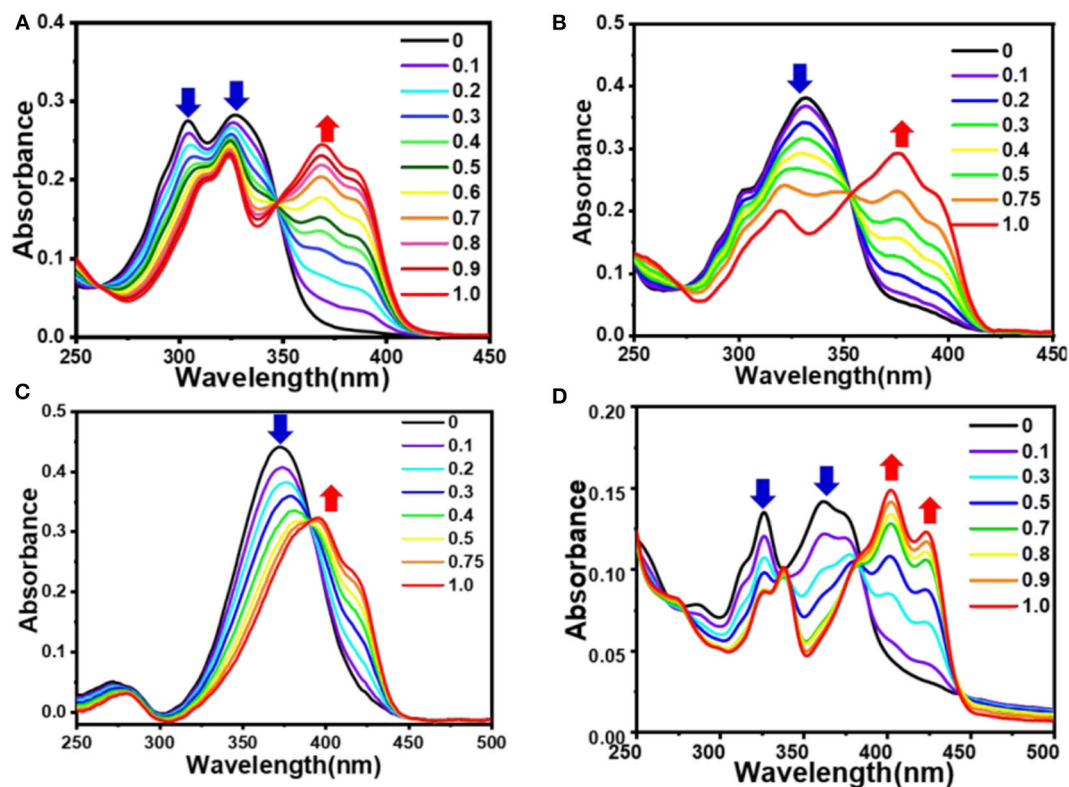


FIGURE 3 | Absorption spectra of **1** (A), **2** (B), **3** (C), **4** (D) (10 μ M) upon the addition of Al³⁺(0-1 eq.) in 0.3% DMSO/bis-tris buffer solution (PH = 7.4).

347.0567), [AlNO₃·(3-H)]⁺ (calcd = 388.1196), and [AlNO₃·(4-H)]⁺ (calcd = 367.0618) can be clearly observed when an excess amount of Al³⁺ were added to **1-4** aqueous solutions, suggesting a 1:1 Ligand-Al³⁺ binding stoichiometry (Figure 4). It can be seen from the results that each sensor was combined to an aluminum atom with a nitrate.

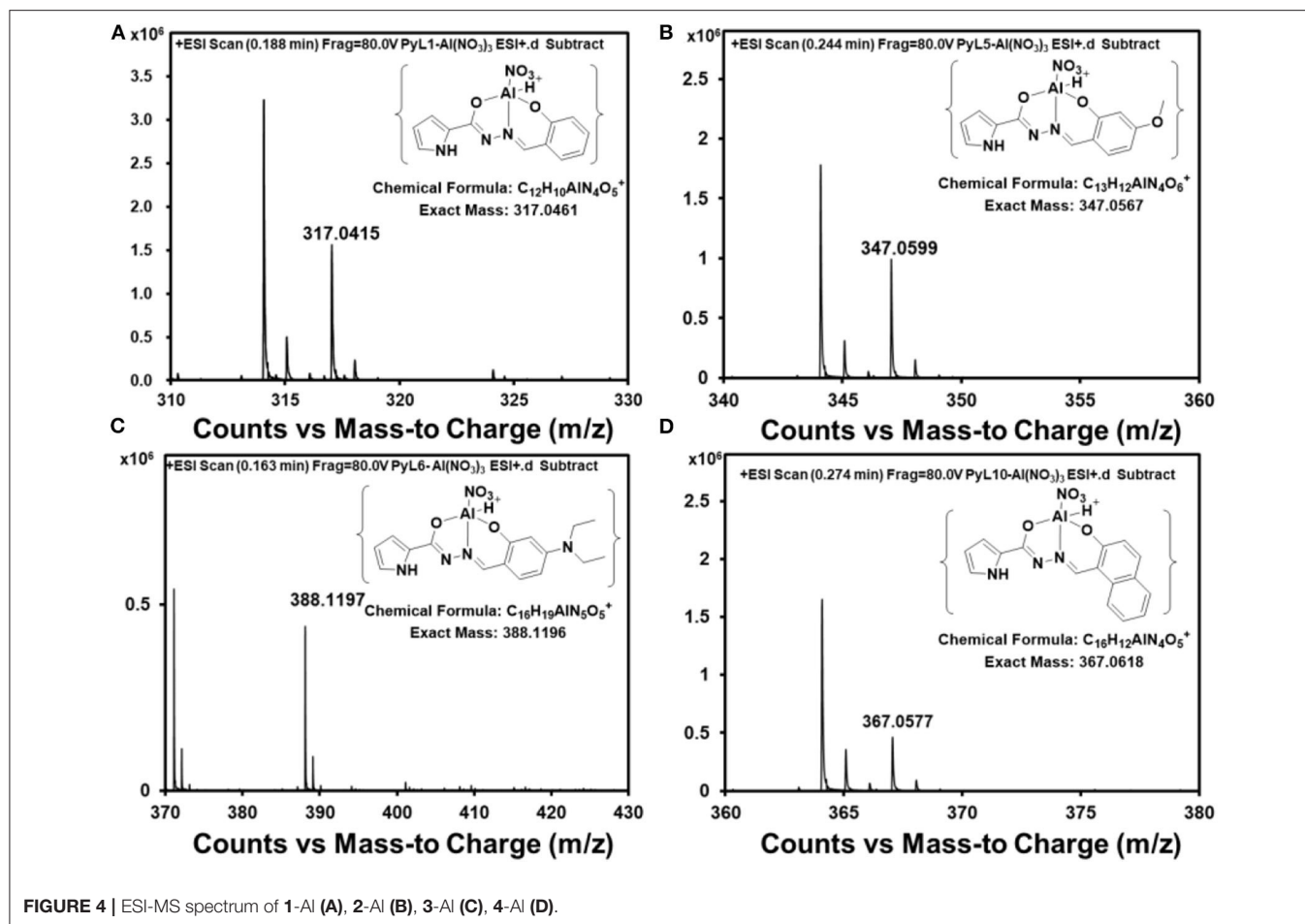
¹H NMR Titrations

In order to further study the absorption and fluorescence phenomena of the sensors, ¹H NMR titration was performed by adding Al³⁺ to sensor **3** (0.5 mM in DMSO-*d*₆ solution). Firstly, ¹H-¹H COSY NMR spectrum of sensor **3** was performed assign the chemical shift of the hydrogen atoms (Supplementary Figure 14). The chemical shift of N-H(H1) on the pyrrole ring was 11.69 ppm. The chemical shift of N-H (H5) was 11.40 ppm, and the chemical shift of hydroxyl O-H (H10) on the benzene ring was 11.39 ppm. After adding Al³⁺ to the sensor **3** by 0.5 equivalent, it can be seen that the ¹H NMR spectrum significantly changed (Figure 5). The chemical shift signals of N-H (H5) on the hydrazide group and O-H (H10) of the hydroxyl group on the benzene ring gradually weakened. After the addition of Al³⁺ increasing to 1 equivalent, the shift signals of H5 and H10 disappeared completely. This also verified that the binding stoichiometry of **3** to Al³⁺ was 1:1. By testing the ¹H-¹H COSY NMR spectrum of **3**-Al³⁺ (Supplementary Figure 15), the signal peaks of each hydrogen of the titration product

can be assigned. Through the titration process, we can observe that the chemical shift of H1 migrates from 11.69 ppm to low field 12.23 ppm, H6 chemical shift from 8.37 ppm to high field 8.26 ppm, H2, H3, H4, H7, H8, H9 chemical shift from 6.20, 6.95, 7.00, 7.21, 6.30, and 6.15 ppm to 6.38, 7.20, 7.32, 7.23, 6.26, and 6.00 ppm. The disappearance of the strong N-H spike indicates that it participates in the enol interconversion of the carbonyl group, and the disappearance of the proton peak of phenol-OH indicates the interaction between Al³⁺ and phenol-OH. The overall change of the ¹H NMR spectrum indicates that Al³⁺ and **3** are complexed and coordinated through the O atom of the carbonyl group, the azomethine-N atom, and the phenolic-OH oxygen atom.

Fluorescence Studies

Fluorescence emission studies were conducted to check the selectivity of **1-4** for various metal ions (Na⁺, K⁺, Ag⁺, Mg²⁺, Ca²⁺, Hg²⁺, Pb²⁺, Cd²⁺, Mn²⁺, Ni²⁺, Co²⁺, Cu²⁺, Zn²⁺, Fe²⁺, Fe³⁺, Cr³⁺, and Al³⁺) (Figure 6, Supplementary Figure 19). After adding the Al³⁺ aqueous solution, the fluorescence intensity of the system was significantly enhanced. However, metal complexes of **1-4** still showed weak fluorescent emission with the addition of other kinds of metal ions. In order to see the fluorescence changes more intuitively, we prepared multiple **1-4** samples with different metal ions. After the addition of Al³⁺ ions, Al³⁺ complexes of **1-4** emitted strong fluorescence



under the irradiation of an UV lamp. Compared with 1-4, the fluorescence intensity of their Al³⁺ complexes had changed significantly, however, there is no obvious change of fluorescence intensity when other metal ions were added to 1-4 (Figures 7, 8, Supplementary Figure 20). Therefore, sensors 1-4 are highly selective for the detection of Al³⁺.

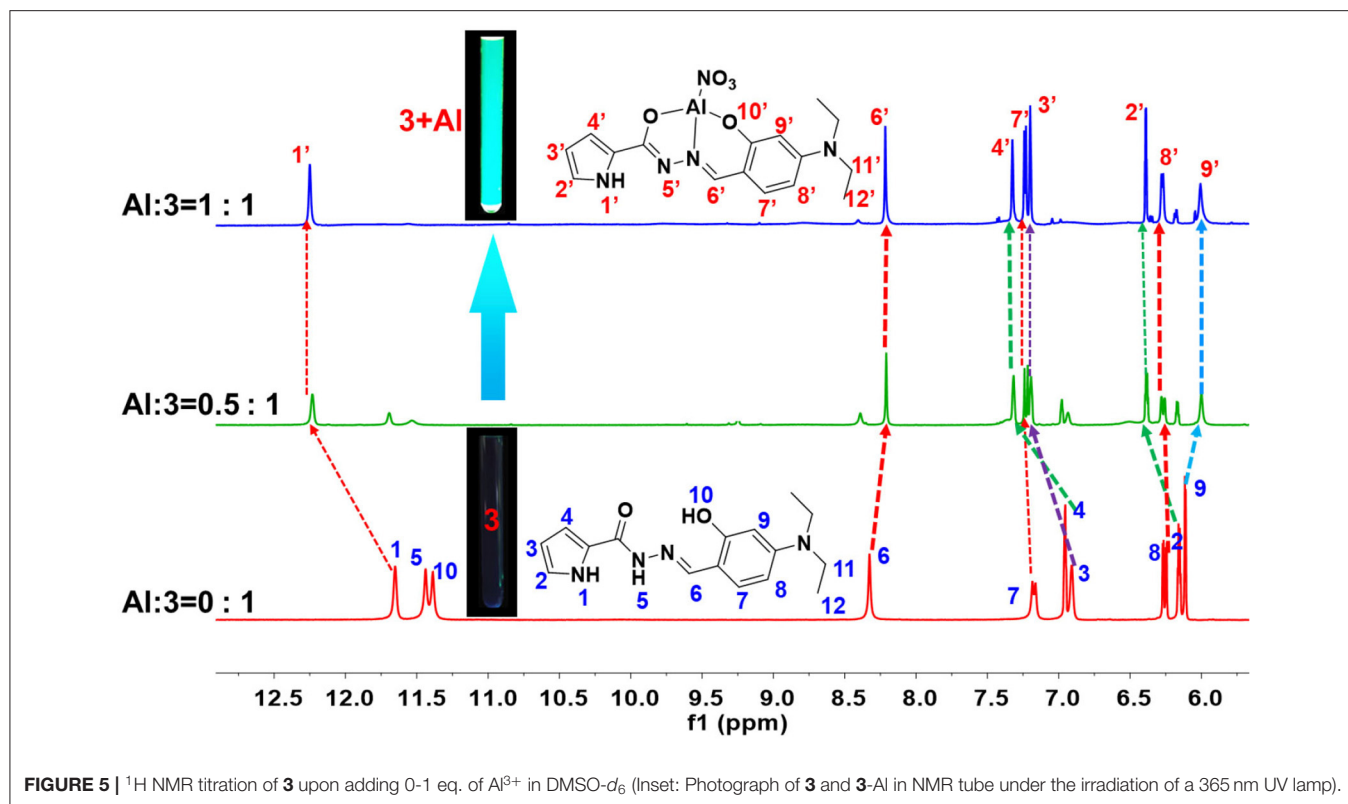
The fluorescence titrations of sensors 1-4 were conducted with increasing amounts of Al³⁺ (Figure 8). It shows that with the addition of Al³⁺ ions (0-1 eq), the fluorescence intensity of 1-4 increased linearly at 446, 448, 453, and 480 nm, respectively. Due to the PET effect and ESIPT processes, ligands 1-4 emit very weak fluorescence. The fluorescence quantum yields of 1-4 (1 μM) with and without Al³⁺ are shown in Table 1. The quantum yields of 1-4 are 0.012, 0.015, 0.011, and 0.042. The quantum yields of 1-Al-4-Al are 0.199, 0.314, 0.315, and 0.093, respectively. The quantum yields changed significantly before and after the sensors 1-4 binding to Al³⁺. Especially sensors 2 and 3, where the fluorescence quantum yield was enhanced by more than 20 times.

In order to verify the preferential selectivity of 1-4 for Al³⁺, various competition experiments were conducted to interfere with metal ions. As shown in Supplementary Figure 21, most of the metal ions have little influence on the detection of Al³⁺ by the detectors 1-4, and only a small part of the metal ions have

influence on the Al³⁺ detection process. Hg²⁺, Cu²⁺, Fe²⁺, and Fe³⁺ have weak effects on the detection process accompanied by a decrease in fluorescence intensity. The interference to Hg²⁺, Cu²⁺, Fe²⁺, and Fe³⁺ may be caused by their intrinsic quenching properties to fluorescence (Jeong et al., 2017).

Theoretical Calculation

In order to more clearly understand the spectral change behavior among 1-4, TD-DFT calculation was operated based on B3LYP/6-31G(d). From TD-DFT data, HOMO and LUMO energy levels and the corresponding electron cloud distribution map of each compound were obtained. HOMO energy levels of 1-4 were -5.65, -5.38, -4.90, and -5.38 eV, and the LUMO energy levels were -1.48, -1.28, -1.08, and -1.63 eV (Figure 9, Supplementary Tables 2-5). Therefore, through the formula $E_{\text{gap}} = E_{\text{LUMO}} - E_{\text{HOMO}}$, it is easy to obtain the HOMO-LUMO energy gap (E_{gap}) values of 1-4 as 4.17, 4.10, 3.82, and 3.75 eV, respectively. Comparing 2, 3, and 1, it can be seen that after introducing the electron-donating substituents N, N-diethyl and methoxy groups on the benzene ring, the energy levels of HOMO and LUMO had improved, but the increase of HOMO was greater than that of LUMO. Therefore, the E_{gap} of 2, 3 was narrowed. Comparing 4 and 1, it can be seen that after the benzene ring was replaced with a naphthalene ring,



the π -conjugation of the molecule expanded. The LUMO energy level was greatly reduced and the HOMO energy level increased, thus narrowing the E_{gap} . The narrower the E_{gap} of the molecule was, the more favorable it would be for the internal electrons of the molecules to be excited. Thus, a red shift in the absorption spectrum occurred. The E_{gap} gradually becomes smaller from **1** to **4**, and the maximum absorption wavelength in the absorption spectrum obtained by the calculation gradually becomes larger, which coincides with the experiment results (Supplementary Figure 22, Supplementary Table 6).

The possible binding mode of sensors and Al³⁺ has been verified by Job's plot, ESI-MS, and ¹H NMR titration, that is, the sensors and Al³⁺ are combined through a 1:1 coordination ratio. DFT and TD-DFT calculations were conducted to optimize the possible molecular structures of **1**-Al, **2**-Al, **3**-Al, and **4**-Al based on B3LYP/6-31G (d) (Figure 10). From the calculation results, the aluminum atom was coordinated with one N and two O in the ligand, and a nitrate was also connected to the aluminum atom.

From the structure of the sensors **1**-**4**, they are mainly divided into two parts, pyrrolyl hydrazide and salicylaldehyde derivatives. It can be seen that the HOMO orbital electron cloud of **1**-Al is mainly distributed on the ligand π conjugated skeleton, and the LUMO orbital electron distribution is mainly concentrated on the Al atom (Figure 11). Sensors **2**-**4** have the same orbital distribution as **1**. The E_{gap} of sensor **1**-Al is 3.29 eV. The E_{gap} for sensor **2**-Al, **3**-Al, and **4**-Al are 3.23, 3.00, and 2.90 eV, respectively. The E_{gap} has decreased significantly from sensor **1**-**4** to **1**-Al - **4**-Al, indicating the E_{gap} becomes narrower during the combination process of probe and Al³⁺,

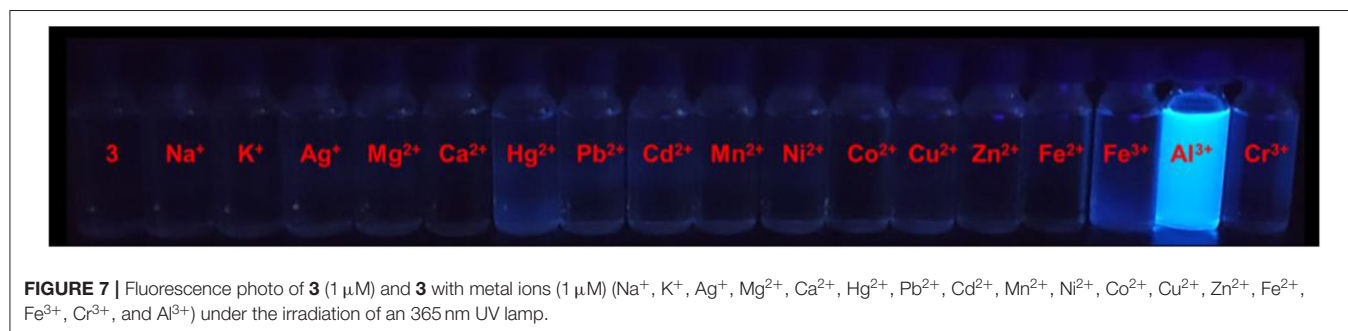
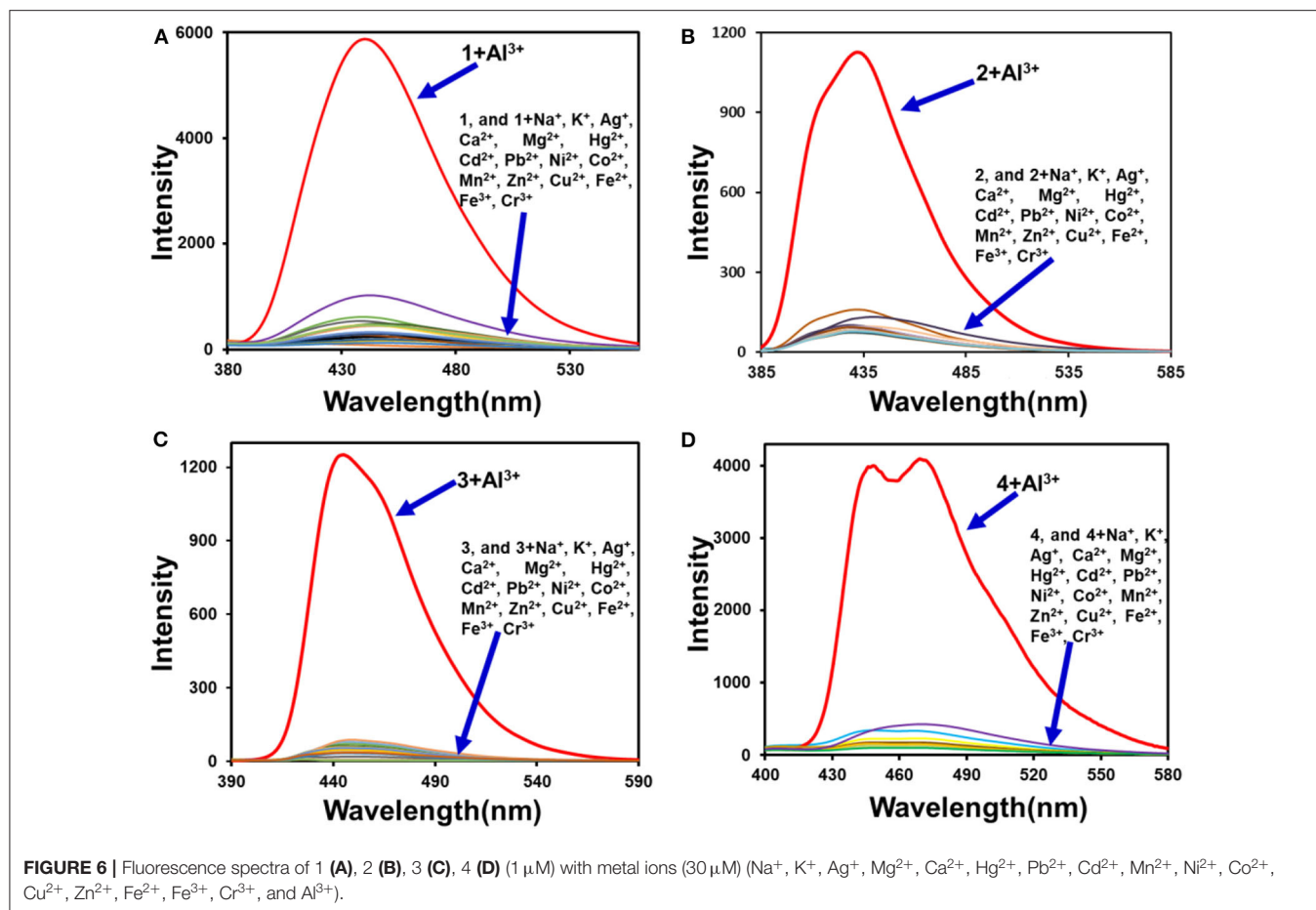
which means that it takes less energy to excite Al complexes than the ligands. As for the experimentally obtained absorption spectrum, it can be seen that the maximum absorption peak red shift occurs after the sensors combined with Al³⁺, it needs lower energy to excite the system to emit fluorescence, which is consistent with the conclusions obtained from the theoretical calculations. The electron cloud of HOMO in sensors-Al³⁺ are mainly distributed on the π conjugate skeleton of the ligand, and the LUMO is mainly concentrated on the central metal Al, the possible reason is mainly the electronic transition caused by LMCT.

“Turn-On” Mechanism of the Sensors

From the side view of the optimized molecular structure diagram (Figures 1, 10), it can be clearly seen that after the sensors bind to the Al³⁺ ion, the coplanarity of the pyrrole ring and the salicylaldehyde ring of the sensors is destroyed, which is not conducive to the charge transfer. The combination of Al atoms and carbonyl oxygen atoms also destroy the enol interconversion of the carbonyl group at the hydrazide structure in the molecule which inhibits the PET and ESIPT effect (Figure 12).

Application of Al³⁺ Test Paper

In order to explore the practical application of the sensors, and make them easily and conveniently applied in life, we have developed test paper for Al³⁺ detection based on **3**. A series of 3.0 μ L 0.5 mM sensor **3** solutions were dropped onto the round filter papers and then dried to obtain blue-violet



fluorescent test papers. To each test paper, 1 μL of various metal ions solutions were added dropwise. After a few seconds, under the ultraviolet light, we could see that the test paper with Al^{3+} emitted a strong blue-green fluorescence (Figure 13). The fluorescence of test papers with the addition of other metal ions were almost unchanged. We also used a paper-made pen which was dipped in Al^{3+} solution to write on a test paper. We could clearly see that the element symbol “Al” emitted strong blue-green fluorescence under the irradiation of a 365 nm UV lamp (Supplementary Figure 24). The simple and easy-to-prepare test paper made by sensor **3** had high selectivity and high sensitivity for identifying Al^{3+} .

CONCLUSIONS

In conclusion, we have synthesized and characterized four novel biosensors (**1-4**) based on pyrrole hydrazone Schiff bases. These sensors have outstanding “turn-on” fluorescence recognition for Al^{3+} ions in aqueous solutions. The binding modes of **1-4** with Al^{3+} were determined by Job’s Plot and ESI-MS spectrometry. The detection limits of **1-4** for Al^{3+} were 53, 45, 42, and 102 nM. ^1H - ^1H COSY NMR spectrum and ^1H NMR titration have also been studied for the interaction between **3** and Al^{3+} . Moreover, DFT and TD-DFT theoretical calculations were used for molecular structure optimization, HOMO, LUMO, and E_{gap}

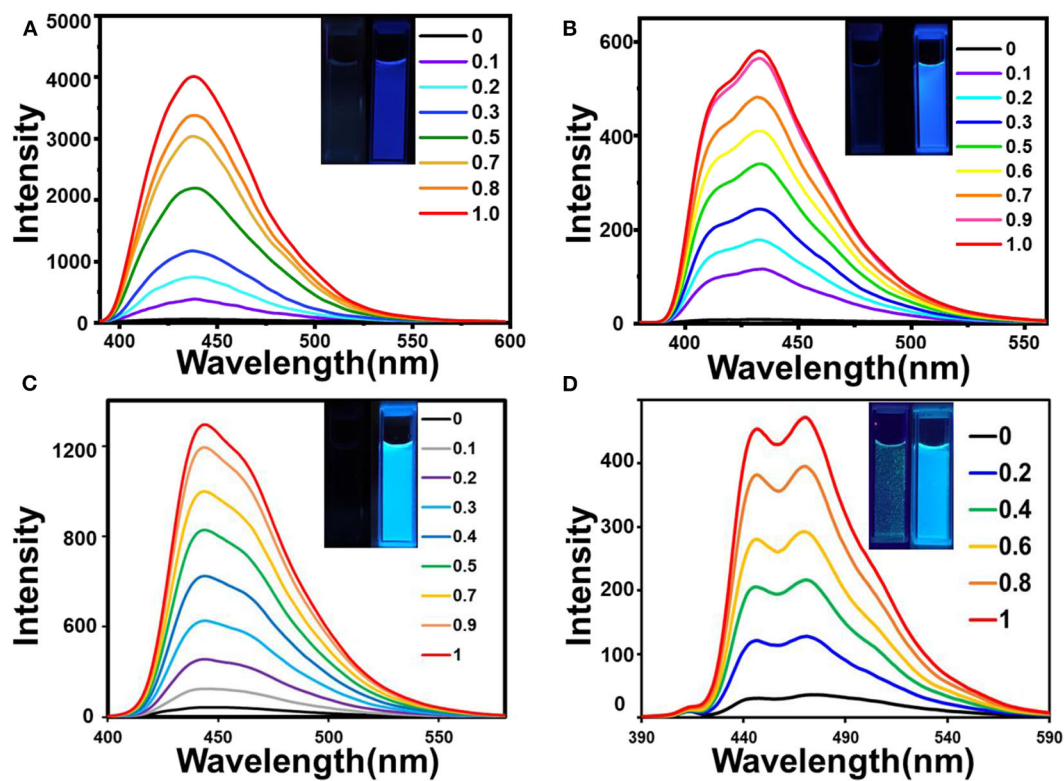


FIGURE 8 | Fluorescence spectra of **1** (A), **2** (B), **3** (C), **4** (D) (1 μ M) upon addition of different equivalent Al³⁺ in 0.03% DMSO/tris-bis buff solution (insets: comparison photos of **1-4** and their Al³⁺ complexes under a 365 nm UV lamp irradiation).

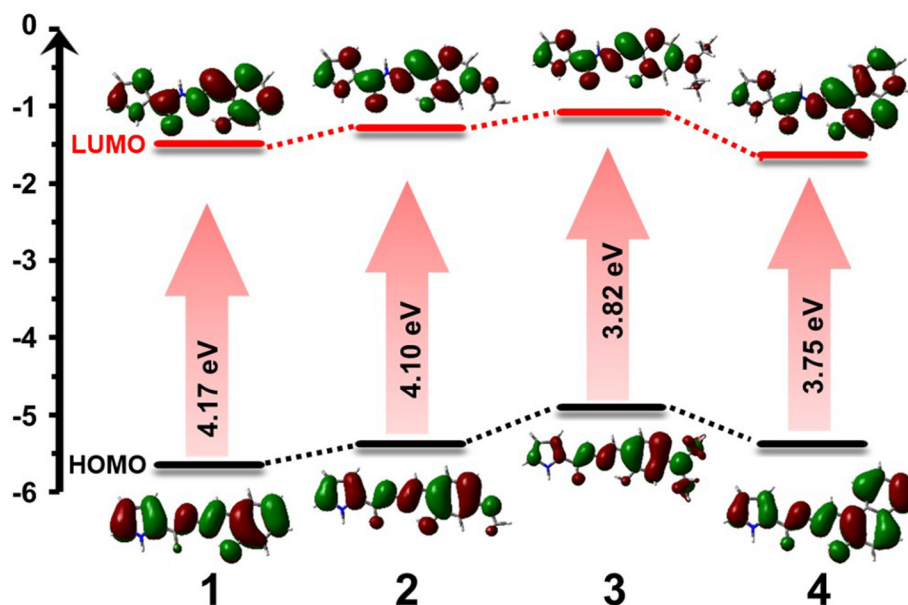


FIGURE 9 | HOMO and LUMO orbital levels and HOMO-LUMO energy gap of **1-4**, calculated with DFT at the B31LYP/6-31G level using Gaussian 09.

calculations and comparisons. It was also used to explain the spectral difference among ligands **1-4**, as well as the change of absorption spectrum before and after the interaction between

1-4 and Al³⁺ and the fluorescence mechanism. The sensing mechanisms were proposed with the PET and ESIPT effect. A high selectivity test strip was developed for Al³⁺ detection-based

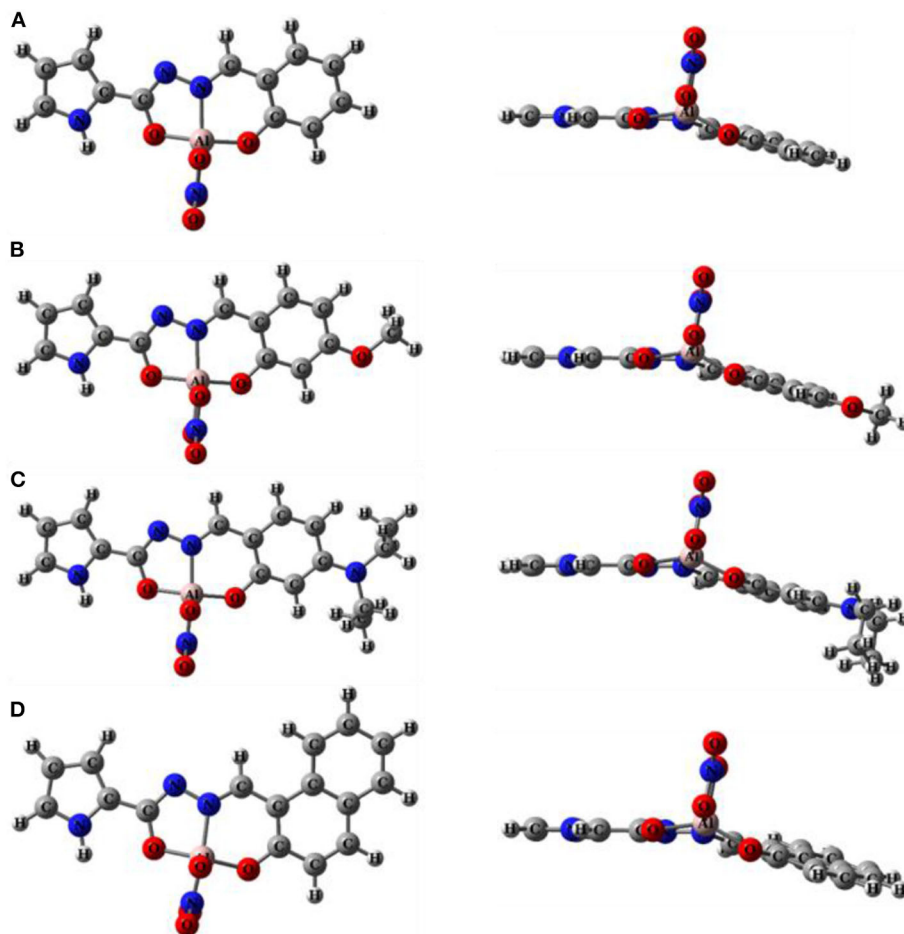


FIGURE 10 | Up view and side view of optimized molecular structure of (A) 1-AI, (B) 2-AI, (C) 3-AI, (D) 4-AI.

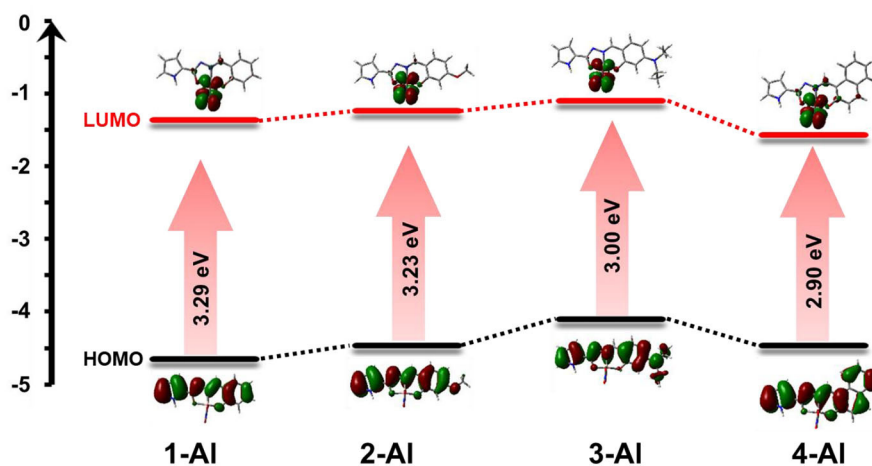


FIGURE 11 | HOMO and LUMO orbital levels and HOMO-LUMO energy gap of 1-AI, 2-AI, 3-AI, and 4-AI, calculated with DFT at the B31LYP/6-31G level using Gaussian 09.

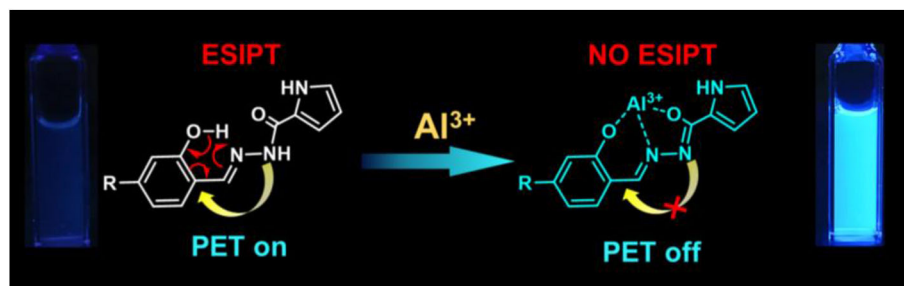


FIGURE 12 | Proposed sensing mechanism of sensors to Al³⁺.

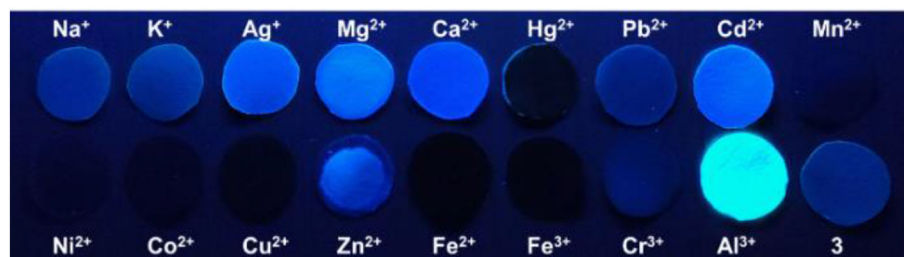


FIGURE 13 | Photograph of detecting metal ions with the test paper of sensor **3**, and test by dropping different ions onto the test paper of sensor **3**. The image was obtained under the irradiation of a 365 nm UV lamp.

sensor **3**. On the basis of the results, we believe that the results will provide an important reference for the development and application in biosensors fields.

DATA AVAILABILITY STATEMENT

The original contributions presented in the study are included in the article/**Supplementary Materials**, further inquiries can be directed to the corresponding author/s.

AUTHOR CONTRIBUTIONS

PW and HL designed the work. PW did the experiment and wrote the manuscript. LL, FM, MK, and HL revised and edited

the manuscript. All authors reviewed the manuscript and have agreed to its publication.

FUNDING

This work was supported by the National Natural Science Foundation of China (No. 21471017).

SUPPLEMENTARY MATERIAL

The Supplementary Material for this article can be found online at: <https://www.frontiersin.org/articles/10.3389/fchem.2020.607614/full#supplementary-material>

REFERENCES

- Aguilar, F., Autrup, H., Barlow, S., Castle, L., Crebelli, R., Dekant, W., et al. (2008). Safety of aluminium from dietary intake - Scientific opinion of the panel on food additives, flavourings, processing aids and food contact materials (AFC). *EFSA J.* 754, 1–34. doi: 10.2903/j.efsa.2008.754
- Balakrishnan, C., Neelakantan, M. A., and Banerjee, S. (2017). A zwitterionic pH responsive ESIPT-based fluorescence “Turn-On” Al³⁺ ion sensing probe and its bioimaging applications. *Sens. Actuator B Chem.* 253, 1012–1025. doi: 10.1016/j.snb.2017.07.030
- Barcelo, J., and Poschenrieder, C. (2002). Fast root growth responses, root exudates, and internal detoxification as clues to the mechanisms of aluminium toxicity and resistance. *Environ. Exp. Bot.* 48, 75–92. doi: 10.1016/S0098-8472(02)00013-8
- Berthon, G. (2002). Aluminium speciation in relation to aluminium bioavailability, metabolism and toxicity. *Coord. Chem. Rev.* 228, 319–341. doi: 10.1016/S0010-8545(02)00021-8
- Boonkitpatarakul, K., Wang, J., Niamnont, N., Liu, B., McDonald, L., Pang, Y., et al. (2015). Novel turn-on fluorescent sensors with mega Stokes shifts for dual detection of Al³⁺ and Zn²⁺. *ACS Sens.* 1, 144–150. doi: 10.1021/acssensors.5b00136
- Chatterjee, N., Maity, S. B., Samadder, A., Mukherjee, P., Khuda-Bukhsh, A. R., and Bharadwaj, P. K. (2016). A chemosensor for Al³⁺ ions in aqueous ethanol media: photophysical and live cell imaging studies. *RSC Adv.* 6, 17995–18001. doi: 10.1039/C5RA23968K
- Das, S., Dutta, M., and Das, D. (2013). Fluorescent probes for selective determination of trace level Al³⁺: recent developments and future prospects. *Anal. Methods* 5, 6262–6285. doi: 10.1039/c3ay40982a

- DeVoto, E., and Yokel, R. A. (1994). The biological speciation and toxicokinetics of aluminium. *Environ. Health Perspect.* 102, 940–951. doi: 10.1289/ehp.94102940
- Dong, H., Luo, M., Wang, S., and Ma, X. (2017). Synthesis and properties of tetraphenylethylene derivative diarylethene with photochromism and aggregation-induced emission. *Dyes Pigm.* 139, 118–128. doi: 10.1016/j.dyepig.2016.11.054
- Frisch M. J., Trucks G. W., Schlegel H. B., Scuseria G. E., Robb M. A., Cheeseman, J. R., et al. (2009). *Gaussian 09, Revision. D.01*. Wallingford, CT: Gaussian, Inc. Available online at: www.gaussian.com
- Fu, J., Li, B., Mei, H., Chang, Y., and Xu, K. (2019). Fluorescent schiff base probes for sequential detection of Al³⁺ and F⁻ and cell imaging applications. *Spectrochim. Acta Part A* 227:117678. doi: 10.1016/j.saa.2019.117678
- Fu, W., Yan, C., Guo, Z., Zhang, J., Zhang, H., Tian, H., et al. (2019). Rational design of near-infrared aggregation-induced-emission-active probes: *in situ* mapping of amyloid- β plaques with ultrasensitivity and high-fidelity. *J. Am. Chem. Soc.* 141, 3171–3177. doi: 10.1021/jacs.8b12820
- Greger, J. L., Sutherland, J. E., and Yokel, R. (1997). Aluminium exposure and metabolism. *Crit. Rev. Clin. Lab. Sci.* 34, 439–474. doi: 10.3109/10408369709006422
- Gupta, A., and Kumar, N. (2016). A review of mechanisms for fluorescent “turn-on” probes to detect Al³⁺ ions. *RSC Adv.* 6, 106413–106434. doi: 10.1039/C6RA23682K
- Hanna, M. L., Tarasow, T. M., and Perkins, J. (2007). Mechanistic differences between *in vitro* assays for hydrazone-based small molecule inhibitors of anthrax lethal factor. *Bioorg. Chem.* 35, 50–58. doi: 10.1016/j.bioorg.2006.07.004
- Hao, L., Qiu, Q., Wang, W., Gu, L., and Li, H. (2016). Fluorescent detection of trace water in methanol based on an Al(III) chemical sensor. *Chin. J. Chem.* 34, 1109–1113. doi: 10.1002/cjoc.201600358
- Huang, Q., Zhang, Q., Wang, E., Zhou, Y., Qiao, H., Pang, L., et al. (2016). A new “off-on” fluorescent probe for Al³⁺ in aqueous solution based on rhodamine B and its application to bioimaging. *Spectrochim. Acta Part A* 152, 70–76. doi: 10.1016/j.saa.2015.07.062
- Hwang, S. M., Kim, M. S., Lee, M., Lim, M. H., and Kim, C. (2017). A single fluorescent chemosensor for multiple targets: the sequential detection of Al³⁺ and pyrophosphate and the selective detection of F⁻ in a near-perfect aqueous solution. *New J. Chem.* 41, 15590–16600. doi: 10.1039/C7NJ03575F
- Jeong, H. Y., Lee, S. Y., Han, J., Lim, M. H., and Kim, C. (2017). Thiophene and diethylaminophenol-based “turn-on” fluorescence chemosensor for detection of Al³⁺ and F⁻ in a near-perfect aqueous solution. *Tetrahedron* 73, 2690–2697. doi: 10.1016/j.tet.2017.03.069
- Jiang, M., Gu, X., Lam, J. W. Y., Zhang, Y., Kwok, R. T. K., Wong, K. S., et al. (2017). Two-photon AIE bio-probe with large Stokes shift for specific imaging of lipid droplets. *Chem. Sci.* 8, 5440–5446. doi: 10.1039/C7SC01400G
- Jiao, Y., Zhang, L., Gao, X., Si, W., and Duan, C. (2020). A cofactor-substrate-based supramolecular fluorescent probe for the ultrafast detection of nitroreductase under hypoxic conditions. *Angew. Chem. Int. Ed.* 59, 6021–6027. doi: 10.1002/anie.201915040
- Kim, S., Noh, J. Y., Kim, K. Y., Kim, J. H., Kang, H. K., Nam, S. W., et al. (2012). Salicylimine-based fluorescent chemosensor for aluminium ions and application to bioimaging. *Inorg. Chem.* 51, 3597–3602. doi: 10.1021/ic2024583
- Kong, J., He, C., Zhang, X., Meng, Q., and Duan, C. (2014). Rhodamine based colorimetric and fluorescent probe for recognition of nucleoside polyphosphates through multi-hydrogen bond. *Dyes Pigm.* 101, 254–260. doi: 10.1016/j.dyepig.2013.10.002
- Krejpcio, Z., and Wojciak, R. W. (2002). The influence of Al³⁺ ions on pepsin and Trypsin activity *in vitro*. *Pol. J. Environ. Stud.* 11, 251–254. Available online at: <http://www.pjoes.com/The-Influence-of-Al-3-Ions-on-Pepsin-r-and-Trypsin-Activity-in-Vitro,87450,0,2.html>
- Kumawat, L. K., Mergu, N., Asif, M., and Gupta, V. K. (2016). Novel synthesized antipyrene derivative based “naked eye” colorimetric chemosensors for Al³⁺ and Cr³⁺. *Sens. Actuator B Chem.* 231, 847–859. doi: 10.1016/j.snb.2016.03.062
- Li, C. Y., Zhou, Y., Li, Y. F., Zou, C. X., and Kong, X. F. (2013). Efficient FRET-based colorimetric and ratiometric fluorescent chemosensor for Al³⁺ in living cells. *Sens. Actuator B Chem.* 186, 360–366. doi: 10.1016/j.snb.2013.06.039
- Li, T., Fang, R., Wang, B., Shao, Y., Liu, J., Zhang, S., et al. (2014). A simple coumarin as a turn-on fluorescence sensor for Al(III) ions. *Dalton Trans.* 43, 2741–2743. doi: 10.1039/C3DT52414K
- Li, X., Gao, X., Shi, W., and Ma, H. (2014). Design strategies for water-soluble small molecular chromogenic and fluorogenic probes. *Chem. Rev.* 114, 590–659. doi: 10.1021/cr300508p
- Li, Z., Ren, M., Wang, L., Dai, L., and Lin, W. (2020). Development of a red-emissive two-photon fluorescent probe for sensitive detection of beta-galactosidase *in vitro* and *in vivo*. *Sens. Actuator B Chem.* 307:127643. doi: 10.1016/j.snb.2019.127643
- Liao, Z. C., Yang, Z. Y., Li, Y., Wang, B. D., and Zhou, Q. X. (2013). A simple structure fluorescent chemosensor for high selectivity and sensitivity of aluminium ions. *Dyes Pigm.* 97, 124–128. doi: 10.1016/j.dyepig.2012.12.017
- Liu, B., Wang, P. F., Chai, J., Hu, X. Q., Gao, T., Chao, J. B., et al. (2016). Naphthol-based fluorescent sensors for aluminium ion and application to bioimaging. *Spectrochim. Acta Part A* 168, 98–103. doi: 10.1016/j.saa.2016.06.002
- O’Boyle, N. M., Tenderholt, A. L., and Langner, K. M. (2008). cclib: a library for package-independent computational chemistry algorithms. *J. Comp. Chem.* 29, 839–845. doi: 10.1002/jcc.20823
- Pawel, D., Zieliński, T. G., and Jurczak, J. (2009). Bishydrazide derivatives of isoindoline as simple anion receptors. *J. Org. Chem.* 74, 1525–1530. doi: 10.1021/jo802288u
- Sahana, A., Benerjee, A., Lohar, S., Banik, A., Mukhopadhyay, S. K., Safin, D. A., et al. (2013). FRET based tri-color emissive rhodamine-pyrene conjugate as an Al³⁺ selective colorimetric and fluorescence sensor for living cell imaging. *Dalton Trans.* 42, 13311–13314. doi: 10.1039/c3dt51752g
- Sharma, S., Dubey, G., Sran, B. S., Bharatam, P. V., and Hundal, G. (2019). Fabrication of a Hydrazone-based Al(III)-selective “turn-on” fluorescent chemosensor and ensuing potential recognition of picric acid. *ACS Omega* 4, 18520–18529. doi: 10.1021/acsomega.9b02132
- Shi, F., Cui, S., Liu, H., and Pu, S. (2020). A high selective fluorescent sensor for Cu²⁺ in solution and test paper strips. *Dyes Pigm.* 173:107914. doi: 10.1016/j.dyepig.2019.107914
- Singh, D. P., Dwivedi, R., Singh, A. K., Koch, B., Singh, P., and Singh, V. P. (2017). A dihydrazone based “turn-on” fluorescent probe for selective determination of Al³⁺ ions in aqueous ethanol. *Sens. Actuator B Chem.* 238, 128–137. doi: 10.1016/j.snb.2016.07.043
- Song, J. B., Wang, P., Yan, L., Hao, L., Khan, M. A., Liu, G. L., et al. (2020). Crystal structures, red-shifted luminescence and iodide-anion recognition properties of four novel D–A type Zn(ii) complexes. *Dalton Trans.* 49, 4358–4368. doi: 10.1039/C9DT04840E
- Tang, Y., Ma, Y., Yin, J., and Lin, W. (2019). Strategies for designing organic fluorescent probes for biological imaging of reactive carbonyl species. *Chem. Soc. Rev.* 48, 4036–4048. doi: 10.1039/C8CS00956B
- Valeur, B., and Leray, I. (2000). Design principles of fluorescent molecular sensors for cation recognition. *Coord. Chem. Rev.* 205, 3–40. doi: 10.1016/S0010-8545(00)00246-0

Conflict of Interest: The authors declare that the research was conducted in the absence of any commercial or financial relationships that could be construed as a potential conflict of interest.

Copyright © 2020 Wang, Liu, Meng, Khan and Li. This is an open-access article distributed under the terms of the Creative Commons Attribution License (CC BY). The use, distribution or reproduction in other forums is permitted, provided the original author(s) and the copyright owner(s) are credited and that the original publication in this journal is cited, in accordance with accepted academic practice. No use, distribution or reproduction is permitted which does not comply with these terms.